Construction and Building Materials 64 (2014) 222–230

Contents lists available at ScienceDirect

Construction and Building Materials

journal homepage: www.elsevier.com/locate/conbuildmat

Pore-scale modelling of 3D moisture distribution and critical saturation in cementitious materials

Mingzhong Zhang [a,b], Kaiming Xu [c,*], Yongjia He [d,e], Andrey P. Jivkov [a,b]

[a] Modelling and Simulation Centre, School of Mechanical, Aerospace and Civil Engineering, The University of Manchester, Manchester M13 9PL, UK
[b] Research Centre for Radwaste and Decommissioning, The University of Manchester, Manchester M13 9PL, UK
[c] Faculty of Architectural, Civil Engineering and Environment, Ningbo University, Ningbo 315211, China
[d] State Key Laboratory of Silicate Materials for Architectures (Wuhan University of Technology), Wuhan 430070, China
[e] School of Materials Science and Engineering, Wuhan University of Technology, Wuhan 430070, China

HIGHLIGHTS

- Macroscopic properties derived from microstructure and pore-scale principles.
- Lattice Boltzmann model developed to account for liquid–gas–solid interactions.
- 3D microstructure obtained from high-resolution micro-CT images.
- Effect of microstructure on moisture distribution estimated quantitatively.
- Predicted critical moisture content in very good agreement with experimental data.

GRAPHICAL ABSTRACT

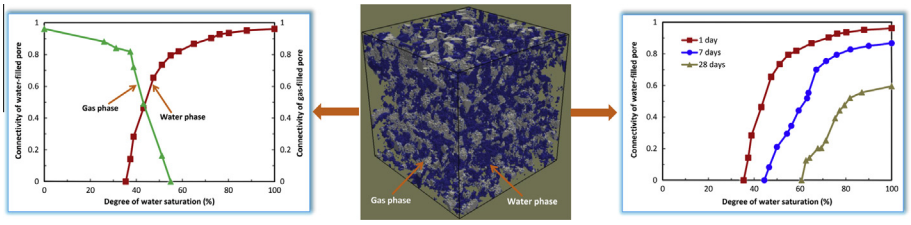

ARTICLE INFO

Article history:
Received 6 February 2014
Received in revised form 1 April 2014
Accepted 4 April 2014

Keywords:
Moisture distribution
Critical saturation
Connectivity
Microstructure
Lattice Boltzmann method

ABSTRACT

The understanding and prediction of moisture distribution and critical moisture content above which fluid and ion transport can occur in porous media is of significant technological importance. A novel computational methodology for simulating moisture distribution and calculating critical content in 3D images of microstructures is presented. The method accounts for the liquid–gas interaction and liquid/gas–solid interaction at the pore scale. Microstructures of cement pastes at different curing ages, obtained by high-resolution X-ray micro-computed tomography, are analyzed. The equilibrium moisture distribution in the 3D microstructures is acquired. The degree of connectivity of the liquid and gas phases is calculated as a function of water saturation level. The critical water saturation for each phase is obtained. It is shown that the moisture distribution and connectivity of each phase depend strongly not only on the degree of water saturation but also on the structures of the pore space and the solid phase. The critical water saturation increases with the decrease of porosity. The results from the simulations are in very good agreement with the experimental data reported in the literature. The proposed methodology is applicable to image-based modelling of all porous media.

1. Introduction

Porous materials, such as concrete, rocks and soils, are usually subjected to cyclic drying–wetting actions by wind, sunlight, rain/snow fall, etc., and are rarely in a state of full saturation in practice. The three-dimensional distribution of moisture in these unsaturated porous media controls a number of physical processes that impact their performance in technological applications, e.g. the durability of cementitious materials, the yield in hydrocarbon recovery, and the containment of hazardous wastes [1]. For instance, the shrinkage of cementitious materials is associated

* Corresponding author. Tel.: +86 (0) 21 34538082.
E-mail address: km.xu@live.com (K. Xu).

http://dx.doi.org/10.1016/j.conbuildmat.2014.04.080
0950-0618/

with the moisture distribution and its evolution within the materials. In order to predict accurately the local shrinkage strains and eventually the shrinkage-induced stresses in cementitious materials, it is necessary to determine the moisture distribution in the first place [2]. Freeze–thaw deterioration is a common cause of damage to concrete in cold climates. Besides the number of cycles of freezing and thawing, and the exposure conditions, the rate of this deterioration depends also on the content and spatial distribution of water in the pore structure of cementitious materials [3]. The prediction of moisture distribution is an essential starting point to assess the damage caused by cyclic freezing and thawing of these materials. The ingress of aggressive species (e.g., chloride and sulphate ions, carbon dioxide, etc.) is the main cause for chemical deterioration with effect on the durability of cementitious materials. The transport of such ions and carbon dioxide in partially saturated cementitious materials is markedly affected by the moisture distribution in the porous network. As shown in Fig. 1, ions can diffuse or electro-migrate only through the liquid containing pores of the network, while carbon dioxide can diffuse only through the gas containing pores. Due to the presence of gas and liquid phases, the diffusion rates of ions and carbon dioxide depend on the degree of saturation and as one grows the other could diminish. In theory, there exists a critical saturation, which is determined as the minimum water saturation degree necessary for the existence of a connected pathway allowing the transport of ionic species. Hence, an understanding of moisture distribution and critical moisture content is crucial to estimate the transport properties and to assess the durability of cementitious materials. Over the past few years, some experimental and computational studies of the moisture distribution and critical moisture level in unsaturated cementitious materials have been reported.

Experimentally, there are several existing methods for measuring liquid phase moisture in cementitious materials, such as nuclear magnetic resonance (NMR) [4], gamma ray, X-ray or neutron radiography (NR) [5], micro-wave spectroscopy [6] and Fourier transform near-infrared (FT-NIR) spectroscopy [7]. There methods can provide direct information on the 2D moisture content profile but not the 3D distribution of moisture within the specimen. In regard of the critical degree of saturation, it was mainly derived from the transport properties such as chloride diffusivity and gas permeability in unsaturated cementitious materials at various moisture levels or relative humidity (RH). Climent et al. [8] measured the chloride diffusion coefficient through unsaturated concrete by means of an innovative test method based on an instantaneous deposition of chloride ion due to the interaction of the concrete surface with the products of combustion of PVC. They reported critical water saturation in the range of 30% to 40%. With the method proposed by Climent et al. [8], de Vera et al. [9] investigated the chloride diffusion coefficient in partially saturated concrete taking into account chloride binding. They reported a critical water saturation of around 33% for transport of chloride ions, which corresponds to RH = 54%. Care and Derkx [10] measured the gas permeability of cement pastes with water-to-cement (w/c) ratios of 0.2, 0.35, 0.45 and 0.6 against the degree of water saturation. They found that the gas did not permeate when the saturation degree reached approximately 82%. Åhs et al. [11] investigated the critical moisture level for unsaturated transport of ions in cementitious materials using electrochemical impedance spectroscopy (EIS) and pointed out that the critical water saturation for ion transport was less than 78% RH. Some of these experimental results are not in agreement with each other, which can be attributed to the difficulty of maintaining a constant water saturation degree of specimens during the tests, and to the dependence of results on the complex microstructure of cementitious materials [10,12,13]. In addition, the tests are usually time-consuming. Therefore, the experimental study of 3D moisture distribution and critical saturation in cementitous materials is still quite challenging.

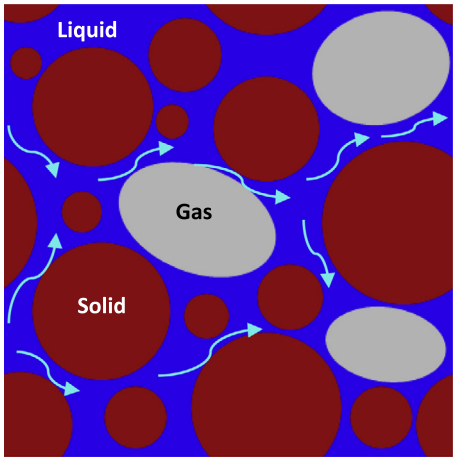

Fig. 1. Schematic illustration of ion transport in the partially saturated porous medium.

With regard to modelling and simulation, Janssen et al. [14] studied the moisture transfer in cement mortar joints with the sharp-front model and X-ray projection method. However, only 2D moisture content profile was obtained. Martys [1] proposed a multi-component lattice Boltzmann model to simulate the moisture distribution in two partially saturated porous materials consisting of overlapping and non-overlapping uniform sized spheres, respectively. A critical saturation of liquid phase of 33% was found. However, the used lattice Boltzmann model only yields the liquid–gas mixture with a density ratio of less than 58, which is much lower than the density ratio of water–gas system (1000/1.29 = 775) in cementitious materials. Moreover, the generated porous media are too simple and cannot represent the complex microstructure of cementitious materials.

The main purpose of this paper is to present a pore-scale modelling of 3D distribution of moisture (a mixture of liquid and gas phases) in cementitious materials with various levels of water saturation accounting for microstructure and to estimate the corresponding critical degree of water saturation. A novel multiphase lattice Boltzmann model is developed and applied to simulate the interactions between liquid, gas and solid phases in the 3D microstructure of cement pastes derived from high-resolution X-ray micro-computed tomography (micro-CT). The 3D distribution of moisture in a state of equilibrium in cement paste specimens is subsequently obtained. Based on the cluster-labeling algorithm, a Perc3d module is developed to quantify the connectivity of each phase in the porous network against degree of water saturation and to estimate critical saturation content. In the end, the influence of microstructure on the moisture distribution and critical saturation content is investigated in a quantitative manner, the results of which are compared with the experimental data reported in the literature.

2. 3D microstructure of cement paste

The starting point for modelling of 3D distribution of moisture in cement paste is the generation of the cement paste microstructure. In the past few decades, a number of computer-based and experimental techniques have been developed and used to generate or characterize the 3D microstructure of cement paste. The computer-based cement hydration models can be grouped into spherical-based and pixel-based models. Comprehensive surveys

of these models have been given by Ye [15], Dolado and van Breugel [16] and Zhang [17]. These models such as HYMOSTRUC3D [15,18] and CEMHYD3D [19] are able to simulate the hydration process and gradual formation of microstructure of cement paste. With regard to experimental approaches, a series of techniques, such as optical microscope, scanning electron microscope (SEM), mercury intrusion porosimetry (MIP) and micro-CT have been widely applied to characterize the pore structure of cement-based materials. Among these techniques, X-ray micro-CT is a non-destructive technique that can be utilized to capture the 3D microstructure of cement-based materials with high resolutions [20]. The simulated 3D microstructure of hydrating cement paste by HYMOSTRUC3D has been successfully applied to investigation of water permeability [21] and ionic diffusivity in saturated and non-saturated cement-based materials [22,23]. In the present study, X-ray micro-CT is used to acquire the 3D microstructure of cement paste.

The X-ray micro-CT scans were carried out at University of Illinois at Urbana-Champaign (UIUC, USA). ASTM type I Portland cement was used. The w/c ratio of the cement paste specimen was 0.5. Specimens were prepared in 250 μm plastic tubes using a syringe. The specimens were stored under standard curing conditions and scanned at 1, 7 and 28 days. A detailed description of the X-ray micro-CT test is given in [20].

In the reconstruction process, 8-bit gray scale was selected to express the signal intensity of the components detected by the CCD camera, the value of which is ranging from 0 (black) to 255 (white). The image resolution was 0.5 μm/voxel. Fig. 2 shows the micro-CT image of a cylinder region with 200 μm in diameter and 100 μm in thickness extracted from the reconstructed 3D image of the 7-day old cement paste. From Fig. 2, some features of different phases, i.e. anhydrous cement grains, hydration products and pores can be seen. Anhydrous cement grains with high density are shown in white. Pore space with low density is shown in black. The gray voxels most probably represent hydration products. To identify these three phases, the image segmentation was performed.

On the basis of gray-level histogram, the threshold gray values were determined by the thresholding method. Consequently, pores, hydration products and anhydrous cement grains were identified. It was shown previously that the representative elementary volume (REV) for transport properties in cement paste was $100 \times 100 \times 100\ \mu m^3$ [24]. Therefore, a cubic volume of interest (VOI) of $100 \times 100 \times 100\ \mu m^3$ was extracted from the center of cylinder region; the cement paste is considered to be the most homogeneous in this region. For comparison, the derived microstructures of VOI of cement paste specimens with curing ages of 1 and 7 days are shown in Fig. 3a and b. It can be seen that the original image is converted into a ternary image of blue, light grey and dark red phases, which represent capillary pores, hydration products and anhydrous cement grains, respectively. In addition, the microstructure evolution of cement paste can be observed. As a result of the progress of cement hydration, the comparison shows a decrease in volume fraction of anhydrous cement grains, porosity, and size of pores, and an increase in volume fraction of hydration products. The corresponding pore structures are extracted and shown in Fig. 3c and d. The porosity of the VOI for all specimens with curing ages of 1, 7 and 28 days, which are referred to as WC50D1, WC50D7 and WC50D28 respectively, is listed in Table 1.

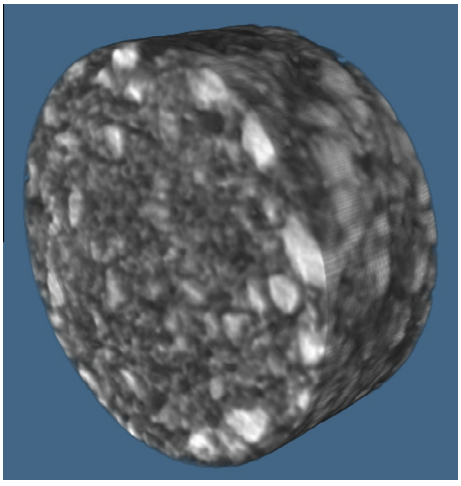

Fig. 2. Micro-CT image of 7-day old cement paste with 200 μm in diameter and 100 μm in thickness (ASTM type I Portland cement with w/c ratio of 0.5).

3. Methodology

3.1. SCMPLBS module: Modified Shan-Chen multiphase lattice Boltzmann model

In order to obtain the 3D moisture distribution in unsaturated cement-based materials, it is essential to simulate the multiphase flow in cement-based materials, which is a challenging task. During the past few years, multiphase lattice Boltzmann models have been proposed, developed and demonstrated their capabilities to model multiphase flow in porous media accounting for the liquid–gas interaction and liquid/gas–solid interaction. Among existing lattice Boltzmann models, the Shan-Chen (SC) model [25,26] is widely used because of its simplicity, ease of implementation and remarkable versatility. It can easily handle fluid phases with different densities, viscosities and wettabilities. However, the original SC model has two major shortcomings: it is not well-established thermodynamically; and the maximum liquid–gas ratio is limited to 58 [27]. These can be overcome by incorporating different kinds of equations of state (EOS) into the original SC model and by changing a parameter named the virtual density of wall. Based on these improvements, a modified SC multiphase lattice Boltzmann simulation (SCMPLBS) module is developed. A brief description of the SCMPLBS module is given below.

At the pore length scale, the fluid is considered as a collection of particles, represented by time-dependent particle distribution functions. These are defined as the probability of finding a particle around a lattice node at a given time. The evolution of the particle distribution functions is described by the Bhatnagar–Gross–Krook (BGK) collision terms [28]:

$$f_i(x + e_i\delta t, t + \delta t) = f_i(x,t) - \frac{1}{\tau}\left[f_i(x,t) - f_i^{eq}(x,t)\right] \tag{1}$$

where f_i and f_i^{eq} are the non-equilibrium and equilibrium particle distribution function at location x at time t; τ is the relaxation time; e_i is the microscopic velocity at location x at time t; and δt is the time step. The relaxation time, τ, is related to the kinematic viscosity of the fluid, υ, via $\upsilon = c_s^2 \cdot (\tau - 0.5)$, where c_s is the lattice speed of sound. The latter is a constant dependent on the choice of lattice and is expressed by $c_s^2 = 1/3 \cdot (\delta x/\delta t)^2$, with lattice-spacing δx and time-step δt measured in lattice unit (lu) and time step (ts) respectively in the lattice Boltzmann method The subscript i represents the number of allowed velocity directions on the lattice. In this study, we use a D3Q19 model, illustrated in Fig. 4, which is a three-dimensional model with nineteen microscopic velocity vectors e_i ($i = 0, 1, \ldots, 18$), listed by Eq. (2).

$$e_i = \begin{bmatrix} 0 & 1 & -1 & 0 & 0 & 0 & 0 & 1 & 1 & 1 & 1 & 0 & 0 & -1 & -1 & -1 & -1 & 0 & 0 \\ 0 & 0 & 0 & 1 & -1 & 0 & 0 & 1 & -1 & 0 & 0 & 1 & 1 & 1 & -1 & 0 & 0 & -1 & -1 \\ 0 & 0 & 0 & 0 & 0 & 1 & -1 & 0 & 0 & 1 & -1 & 1 & -1 & 0 & 0 & 1 & -1 & 1 & -1 \end{bmatrix} \tag{2}$$

For the D3Q19 model, the equilibrium distribution function f_i^{eq} is given by

$$f_i^{eq} = w_i\rho\left[1 + \frac{e_i \cdot \boldsymbol{u}}{c_s^2} + \frac{(e_i \cdot \boldsymbol{u})^2}{2c_s^4} - \frac{\boldsymbol{u} \cdot \boldsymbol{u}}{2c_s^2}\right] \tag{3}$$

where ρ and $\boldsymbol{u}$ are the macroscopic density and velocity respectively, w_i is the weight factor associated with ith direction which is given as $w_i = 1/3$ ($i = 0$), $w_i = 1/18$ ($i = 1, 2, \ldots, 6$) and $w_i = 1/36$ ($i = 7, 8, \ldots, 18$).

In the SC model, the macroscopic local density (mass) $\rho(x,t)$ and velocity $u(x,t)$ of each lattice node are related to the distribution function $f_i(x,t)$ and the force item consisting of fluid–fluid interaction force F_{int}, fluid–solid adhesion force F_{ads} and external force F_g including gravity effects by

$$\rho = \sum_{i=0}^{n} f_i \tag{4}$$

$$\boldsymbol{u} = \frac{1}{\rho}\sum_{i=0}^{n}(f_i \cdot e_i) + \frac{\tau \cdot (F_{\text{int}} + F_{ads} + F_g)}{\rho} \tag{5}$$

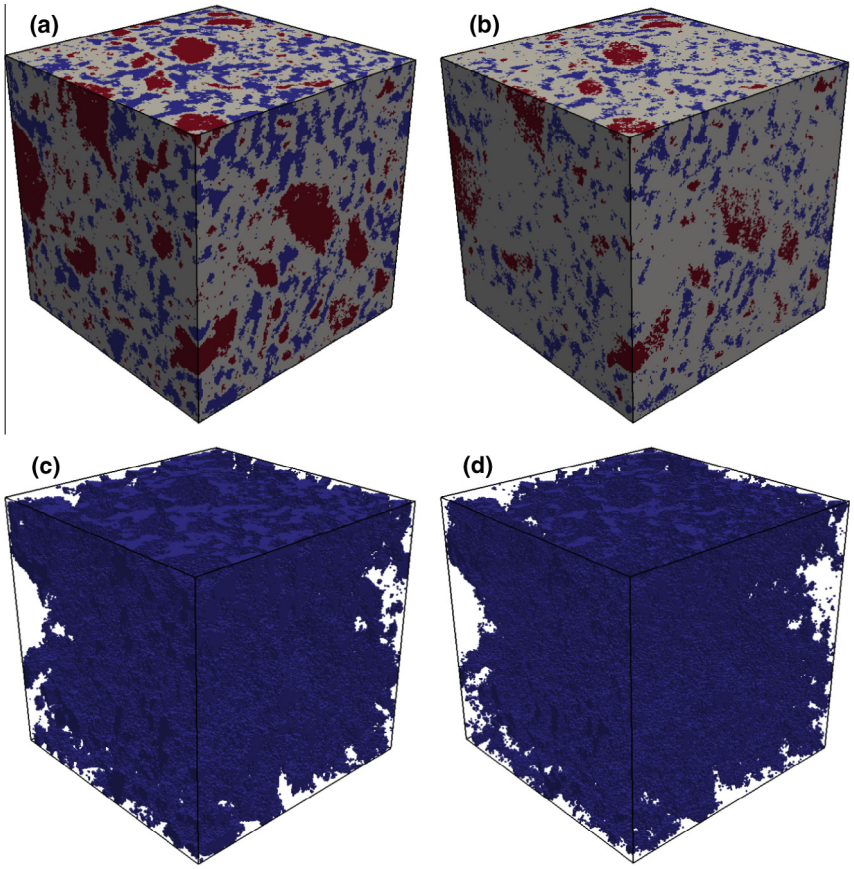

Fig. 3. Computed micro-tomography of cement paste: (a) microstructure of 1-day old cement paste; (b) microstructure of 7-day old cement paste (red region denotes anhydrous cement grains, light grey region represents hydration product and blue region is capillary pore); (c) segmented pore structure of 1-day old cement paste; (d) segmented pore structure of 7-day old cement paste.

Table 1
Porosity of the VOI of specimens at different curing ages.

	Specimens		
	WC50D1	WC50D7	WC50D28
Porosity (%)	27.3	18.9	13.5

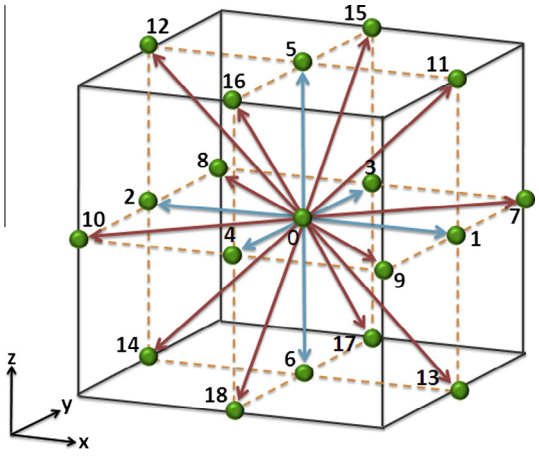

Fig. 4. Lattice velocity direction of the D3Q19 model.

Microscopically, the separation between two phases is the result of fluid–fluid interaction force. In the SC model, the fluid–fluid interaction force F_{int} between the fluid particles at lattice location x and its closest neighboring nodes at time step t is given by [29]

$$F_{\text{int}} = -G\psi(x,t)\sum_{i=1}^{18} w_i\psi(x+e_i,t)e_i \tag{6}$$

where G is the coefficient of attraction between fluid particles, representing the intensity of inter-particle interaction, and Ψ is the so-called "effective mass" which is a function of local density $\Psi(\rho)$. The value of G is negative for attraction and positive for repulsion between particles. The "effective mass" function Ψ directly relates to the interaction force. The forms of Ψ control the detailed nature of the interaction potential and determine the EOS of the fluid system. Ψ is expressed as

$$\psi(\rho) = \sqrt{\frac{2(p-c_s^2\rho)}{c_s^2 g}} \tag{7}$$

In this study, the SC model is modified by replacing the original SC EOS with the Carnahan–Starling (C–S) EOS, which is given as follows

$$p = \rho R_0 T\frac{1+b\rho/4+(b\rho/4)^2-(b\rho/4)^3}{(1-b\rho/4)^3} - a\rho^2 \tag{8}$$

where T denotes the absolute temperature of the gas. In simulations, the constants a, b and R_0 are generally set to 1, 4 and 1, respectively [30].

The adhesion force between liquid/gas phase and solid phase in the SC model F_{ads} is described as

$$F_{ads} = -G\psi(x,t)\sum_{i=1}^{18} w_i\psi(\rho_w)s(x+e_i)e_i \tag{9}$$

where ρ_w is the virtual density of the solid phase which is a free parameter applied to denote different wettability, $s(x+e_i)$ is an indicator function which is set to 1 if the neighboring lattice site $(x+e_i)$ is a solid node and to 0 otherwise. The adhesion force emerges once the neighboring node of a fluid node is solid. By varying the value of ρ_w, the different contact angle between fluid and solid surface can be obtained conveniently.

To validate the SCMPLBS module based on the modified SC model, two benchmark examples, i.e., bubble test and contact angle test, were carried out in a previous work [23]. It was observed that the SCMPLBS module had the capacity to simulate the realistic multiphase flow phenomena such as liquid–gas phase

segmentation (Laplace's law) and variable wettability (contact angle). The SCMPLBS module will be utilized to simulate the moisture distribution in partially saturated cement paste.

3.2. Perc3d module: Degree of pore connectivity

The connectivity is arguably the key pore structure characteristic controlling transport in porous media. In order to estimate the connectivity of the phase of interest (e.g. liquid and gas) in partially saturated cement-based materials, a percolation analysis is performed in this study. Based on the cluster-labeling algorithm proposed by Hoshen and Kopelman [31], an in-house programme, Perc3d, was developed and applied to analyze the connectivity of the water-filled and gas-filled pore network.

In the 3D digital image system, each voxel (except the edge voxels) has six neighbors. The criterion of the connectivity of pore voxels in the 3D digital image system is shown in Fig. 5. On one hand, adjacent voxels are judged as connected voxels when they share a common surface (as shown in Fig. 5a). On the other hand, if adjacent voxels make contact with each other by an edge (as shown in Fig. 5b) or a vertex (as shown in Fig. 5c), they are not connected. The programme scans the whole image system in two steps. A 2D binary image example is shown in Fig. 6a to demonstrate the entire procedure. In the binary image, "0" and "1" represents the solid and pore pixel respectively. Firstly, the scan starts from the left top corner to right bottom corner along the scan direction slice by slice to check the connectivity. If a pore pixel make face-to-face contact with the neighboring pixel (left, top), they are labeled with the same cluster number. If a pore pixel is not connected to any of the neighboring pixels, it is labeled with a different cluster number. After the first step, each pore pixel has a respective cluster, as shown in Fig. 6b. Secondly, the different clusters are checked if the corresponding pixels are connected or not. If they are connected, the clusters are merged into one which assumes the smaller of the two previous indices, as shown in Fig. 6c. The implementation for 3D cases is similar. After the cluster-labeling is complete, the labeled pixels that are not connected to both ends of the specimen (x-, y- and z-axis) are identified as isolated pores. The volume fraction of the labeled pore voxels that are connected to both ends of the specimen is defined as connected porosity.

The degree of pore connectivity is defined as the ratio between the number of voxels in the connected porosity and the total number of pore (labeled) voxels. A degree of pore connectivity of one means that all the pore voxels are interconnected to each other. Inversely, a degree of pore connectivity of zero demonstrates that disconnection happens. The Perc3d module produces a pore network that has a connection to both ends of the specimen. This pore network is assumed to have the most significant contribution to the fluid and ion transport in cement-based materials. By means of cluster-labeling technique, the programme is able to detect how the different pore voxels are connected into a pore network and how many pore voxels are interconnected between one surface and the opposite surface of 3D microstructure.

3.3. Modelling and simulation procedure

The entire modelling and simulation procedure consists of the following three steps.

Step I: Water and gas phases are randomly distributed in the 3D pore network obtained by X-ray micro-CT, subject to a prescribed degree of water saturation. A generator of uniformly distributed random numbers between 0 and 1 is used to assign water or gas to individual pore voxels. As a result, the pore space in the cement paste is saturated with a homogeneous mixture of water and gas phases with a given volume ratio (degree of water saturation). Fig. 7 shows an example of the initial random distribution of water and gas phases with degree of water saturation of 50% in 3D microstructure and pore network of cement paste with curing age of 1 day (the microstructure and pore structure of which are plotted in Fig. 3a and c, respectively).

Step II: The SCMPLBS module, based on the modified Shan-Chen multiphase lattice Boltzmann model, is used to simulate the water–gas and water/gas–solid interactions, and to establish the equilibrium distribution of water and gas phases (moisture) in the hardened cement paste. The physical density ratio between water and gas is 1000/1.29 = 775. Therefore, a suitable value for T, present in Eq. (8), should be chosen in order to meet the requirement of such density ratio of water and gas in lattice Boltzmann units. As shown in the bubble test for a water–gas system [23], a value of $T = 0.585$ yields a density ratio of liquid and gas phases of 0.4152/0.00053 = 783. So, the initial water and gas densities in lattice Boltzmann units are set to be 0.4152 and 0.00053, respectively. In addition, it is commonly assumed that the contact angle between water and solids in cement-based materials is zero. For this reason, the virtual density of solid nodes ρ_w, present in Eq. (9), is set to close the density of the water phase, which results in a zero contact angle and the solid is completely wetted by water [23]. The interaction between water, gas and solid phases is assumed to have reached an equilibrium state once the relative difference of the macroscopic density of water phase in the system at time step t and $(t - 1000)$ calculated by Eq. (4) is less than 10^{-5}.

Step III: The Perc3d module, based on the cluster-labeling algorithm, is used to estimate the degree of connectivity of water-filled and gas-filled pores. The equilibrium distribution of water and gas phases in cement paste with various degree of water saturation obtained from the SCMPLBS module (example in Fig. 7) is regarded as the initial conditions for percolation analysis. On one hand, each gas voxel is converted to a solid-like voxel. Thus, a new domain consisting of water-filled pore voxels, solid-like voxels and solid voxels is created. Using the Perc3d module, the connected and isolated water-filled pore voxels in the new domain are identified, and the connectivity of water-filled pore voxels under various saturation degrees is quantified. Furthermore, the critical degree of saturation at which the water-filled pores become disconnected is obtained. On the other hand, the connectivity of gas-filled pore voxels is estimated in a similar way.

4. Results and discussion

4.1. 3D equilibrium distribution of moisture

Fig. 8a and b show the 3D equilibrium distribution of moisture (i.e., water–gas mixture) in the microstructure and pore network of 1-day old cement paste (as plotted in Fig. 3a and c) with degree of water saturation of 50%. The red region denotes the solid phase which is comprised of anhydrous cement grains and hydration products. The blue region represents the water phase and the light grey region stands for the gas phase. It can be seen that the liquid water covers the surface of the solid phase and tends to fill the pores with smaller size in terms of capillary condensed water. In contrast to liquid water, the gas phase tends to occupy the central region of bigger pores and forms many gas phase clusters, which actually act as obstacles to ion transport and provide possible paths for diffusion of gas, e.g. carbon dioxide and oxygen, in partially saturated cementitious materials.

To clearly demonstrate the distribution of liquid and gases in pore network, the water-filled pores and gas-filled pores are extracted and shown in Fig. 8c and d, respectively. Note that the water-filled pore network is rather complex, consisting of a number of small pores. Because the liquid water lies mostly on the solid surface, the network of water-filled pores is highly dependent on the surface tortuosity of the solid phase. Compared to the water-filled pore network, the gas-filled pore network contains less clusters and has more big pores. The obtained water-filled and gas-filled pore network is used as input to estimate the degree of connectivity, the results of which are presented in the following section.

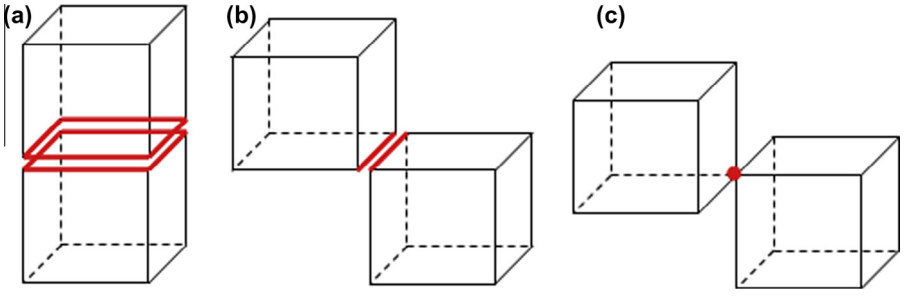

Fig. 5. Possible configurations of adjacent voxels in a 3D image system.

0	1	1	0	0	0	0
0	1	1	0	0	0	0
0	1	0	1	1	0	0
0	1	0	1	1	0	0
1	1	0	0	0	1	0
1	0	0	0	1	1	1
1	0	0	0	1	0	1

(a)

0	1	1	0	0	0	0
0	1	1	0	0	0	0
0	1	0	2	2	0	0
0	1	0	2	2	0	0
3	1	0	0	0	4	0
3	0	0	0	5	4	4
3	0	0	0	5	0	4

(b)

0	1	1	0	0	0	0
0	1	1	0	0	0	0
0	1	0	2	2	0	0
0	1	0	2	2	0	0
1	1	0	0	0	4	0
1	0	0	0	4	4	4
1	0	0	0	4	0	4

(c)

Fig. 6. A 2D example of the implementation of cluster-labeling program: (a) 2D binary image; (b) labeled clusters after first step; (c) labeled clusters after second step.

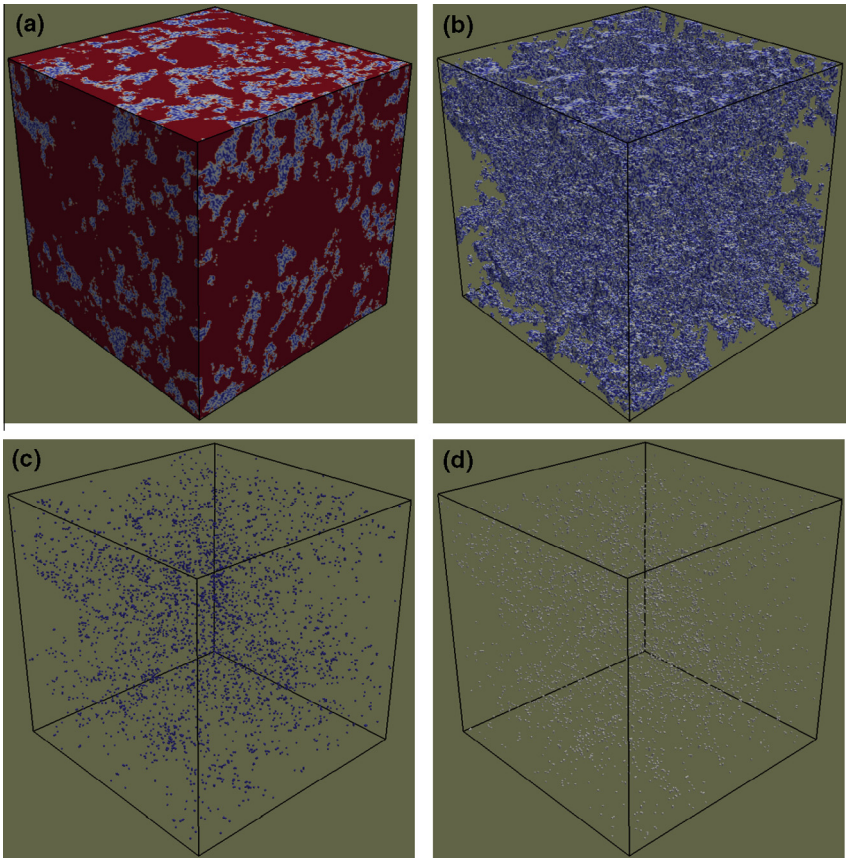

Fig. 7. Initial random distribution of water–gas system with degree of water saturation of 50% in 3D microstructure andpore network of 1-day old cement paste corresponding to Fig. 3a and c (red region is solid phase, blue region denotes water phase and light grey region is gas phase). (For interpretation of the references to color in this figure legend, the reader is referred to the web version of this article.)

4.2. Degree of connectivity

Fig. 9a and b show the continuous water and gas phases, respectively, through the pose space with a saturation of 50%. These correspond to the water-filled and gas-filled pore networks given in Fig. 8. It is observed that most of water-filled pores are interconnected with a degree of connectivity of about 73%. On the contrary, the gas-filled pores are mostly isolated and the corresponding degree of connectivity is only about 16%. The main reason for this is that the liquid water typically forms thin layers along the solid surface, while the gas phase lies in the middle of the pores. When the volume fraction of solid phase is high (in this case, 72.7%) and the degree of water saturation is moderate (here, 50%), the water phase is easier to form a continuous path through the pore space compared to gas phase.

In a similar way, the equilibrium states of moisture distribution in the specimen with different degrees of saturation are derived and the corresponding degrees of connectivity are calculated. Fig. 10 shows the degree of connectivity of the water and gas phases as a function of degree of water saturation for cement paste with curing age of 1 day. It can be seen clearly that there is a strong dependence of degree of connectivity of both phases on the water saturation. The degree of water phase connectivity reduces gradually with reduction in water saturation until around 60%. Below this value it becomes more difficult for the water phase to form a continuous path, since liquid water typically forms a thin film on the solid surface. As a result, the degree of water phase connectivity is reduced rapidly until a saturation of about 34%, below which the water phase through the pore space does not form a percolating network. This degree of water saturation is commonly defined as the critical saturation. The result from our simulations is in a very good agreement with the experimental values reported by Climent et al. [8] and de Vera et al. [9] for the critical water saturation for cementitious materials being around 33%. For the case of gas

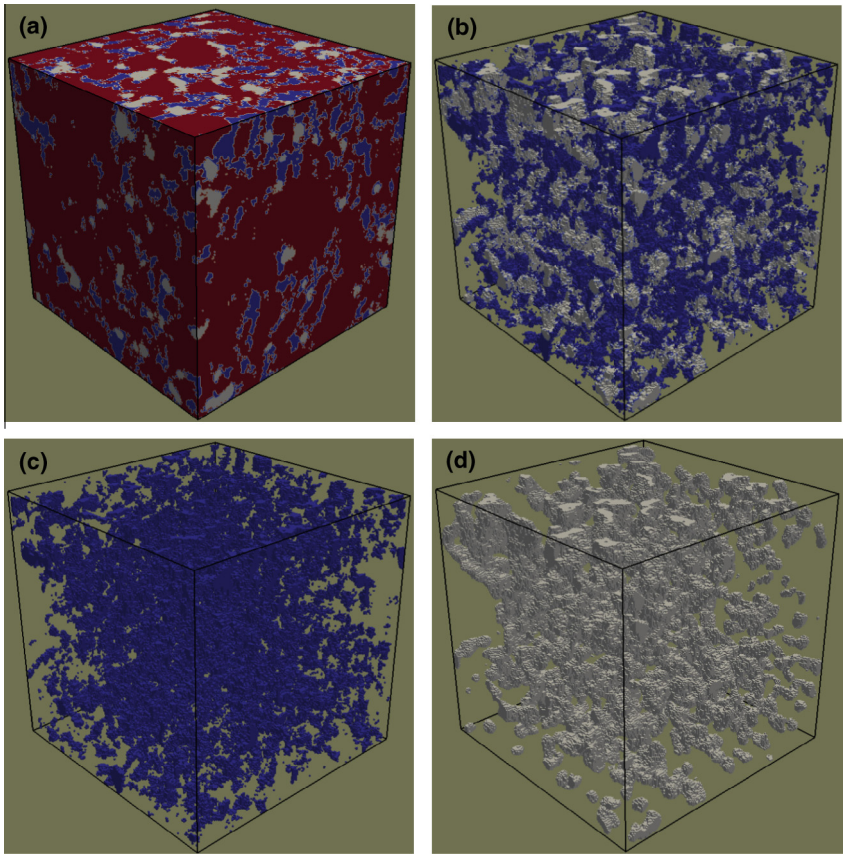

Fig. 8. Equilibrium distribution of moisture in the microstructure and pore network of cement paste with degree of water saturation of 50% corresponding to Fig. 7 (red region is solid phase, blue region denotes water phase and light grey region is gas phase). (For interpretation of the references to color in this figure legend, the reader is referred to the web version of this article.)

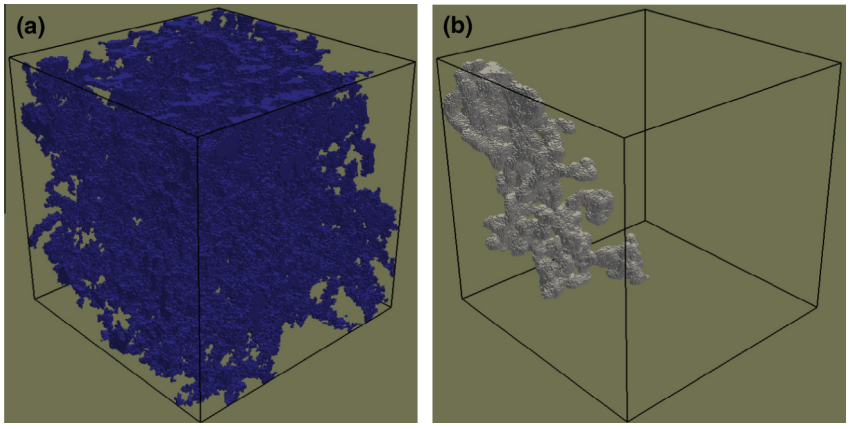

Fig. 9. Continuous network through the pose space with a saturation of 50%: (a) water phase; (b) gas phase.

phase, the degree of connectivity decreases gradually with increasing water saturation until about 34%. This is followed by a rapid decrease with the increase of water saturation and degree of water phase connectivity. At a water saturation of about 55%, the equilibrium gas phase in the pore space becomes disconnected. Above this value there is no effective pathway for gas to diffuse and the existing gas pockets act as isolated obstacles to ion transport in the percolating water phase.

It is worth pointing out that the image resolution might affect the simulation results of percolation since the generated pore structure of a sample with various resolutions would be different. For more details about the influence of image resolution, the reader is referred to [17].

4.3. Influence of microstructure

As shown in the previous two sub-sections, the equilibrium distribution of moisture in partially saturated cementitious materials depends not only on the liquid phase content, i.e. the degree of water saturation, but also on the geometry of the porous network shaped by the distribution of the solid phase. The latter information is included in the 3D microstructure of cementitious materials.

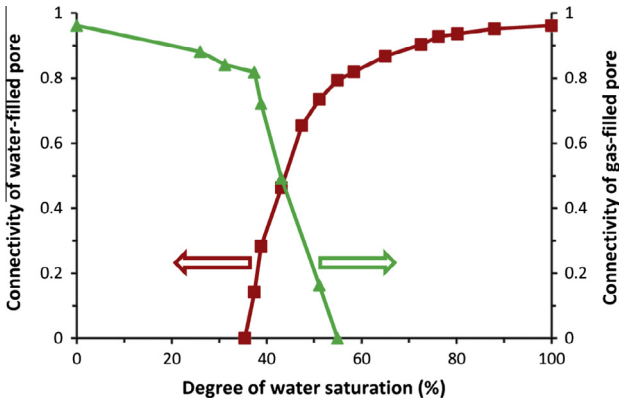

Fig. 10. Degree of connectivity of water-filled and gas-filled pores as a function of water saturation level.

In order to investigate the influence of the microstructure on the water phase connectivity and critical saturation, cement paste specimens with curing ages of 1, 7 and 28 days, i.e. WC5OD1, WC50D7 and WC50D28, obtained by X-ray micro-CT are analyzed. The microstructure and pore structure characteristics of these samples are given in Fig. 3 and Table 1 respectively.

Fig. 11 shows the connectivity of water-filled pore in WC5OD1, WC50D7 and WC50D28 as a function of water saturation degree. Note that at 100% water saturation, there is a significant difference in the degree of pore connectivity at different curing ages. The pore connectivity is reduced from about 96% at 1-day aged (WC50D1) to 87% at 7-days aged (WC50D7) and 60% at 28-days aged (WC50D28) sample. This is attributed to the difference in porosity, pore size distribution and tortuosity of pore network in these specimens. As the degree of water saturation decreases, the connectivity of water phase in all specimens decreases. Eventually the water phase form disconnected thin films along the solid surface so that it no longer percolates. Compared to WC50D1, the decreasing trend of connectivity of water-filled pores for WC50D7 and WC50D28 is more obvious, since they have a lower porosity and a more refined pore network with higher proportion of smaller pores. In the regime of low water saturation, the water phase tends to fill in the smallest pores and the gas phase prefers to occupy the central part of larger pores (as shown in Fig. 8), which leads to a more tortuous water-filled pore network. For WC50D28, this effect is more pronounced, which results in a much more rapid decrease in the connectivity of water-filled pore network as the water saturation decreases compared to WC50D1 and WC50D7. Over the entire range of water saturation, the difference in the connectivity of water phase between WC50D28 and WC50D7 is more noticeable compared to that between WC50D7 and WC50D1.

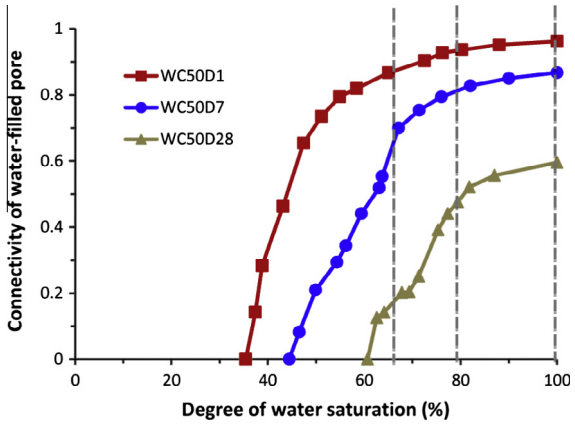

Fig. 11. Degree of connectivity of water-filled and gas-filled pores as a function of degree of water saturation.

From Fig. 11 the critical saturations for WC5OD1, WC50D7 and WC50D28 are found to be 34%, 45% and 61%, respectively. This result indicates that the critical saturation depends strongly on the specimens' microstructures. Specifically, the critical saturation increases with the decrease of porosity and pore size, and the increase of the tortuosity of the pore space. These outcomes are in agreement with the experimental findings by Mercado-Mendoza et al. [13], who measured the chloride diffusion coefficient in unsaturated cement pastes and concretes cast with either Portland cement or blended cement. They argued that the change of chloride diffusivity with degree of water saturation depends critically on the pore structure properties, e.g. porosity and pore size distribution. Our simulations support this argument and show that the structure of the solid phase also plays a significant role.

We define a critical water-filled porosity as the product of the critical saturation and the cement porosity. This is useful for establishing a relation between the connectivity of water-filled pore and porosity. The values of critical water-filled porosity for WC5OD1, WC50D7 and WC50D28 are 9.4%, 8.5% and 8.3%, respectively. Below these values ion transport cannot occur. This result is consistent with the observations of Ye [15] and Zhang et al. [20] that the percolation threshold of the capillary porosity in cementitious materials is about 9% porosity.

It should be mentioned that the above simulations are only compared with the macroscopic experimental data, e.g., critical saturation, due to a lack of available 3D moisture distribution in microstructure from experiments. To further validate the proposed pore-scale modelling scheme, transport properties (e.g. water permeability, chloride diffusivity, gas diffusivity) in partially saturated cementitious materials based on the obtained moisture distribution in this work are needed to estimate and compare with the experimental results recently reported in the literature, e.g. [32,33]. This is a subject of ongoing work and will be presented in a future publication. Furthermore, the obtained equilibrium moisture distribution can be used to analyse the shrinkage-induced cracking in early-age concrete, and freeze–thaw-induced damage in cementitious materials. This will be carried out based on a complementary mechanics model for micro-crack generation and evolution, the recently proposed site-bond model [34,35].

In general, the presented methodology applied to experimentally-acquired 3D images yields results in excellent agreement with macroscopic experiments. This lends confidence in the theoretical basis of the methodology and suggests that it can be used in predictive manner for studies of structure-properties relations. The simulations presented here are constrained to the microstructures formed naturally as the cement paste cures in terms of pore space and solid phase characteristics. Clearly, the methodology can be applied to a larger class of microstructures with different variations of these characteristics, in particular by using synthetic models. This can also reduce the potential bias in the results introduced by the selection of the volumes of interest imaged.

5. Conclusions

Three-dimensional equilibrium distributions of moisture (a mixture of liquid phase and gas phase) in unsaturated cementitious materials have been simulated using a modified Shan-Chen multiphase lattice Boltzmann model. The corresponding evolutions of connectivity of the two phases with the water saturation level have been determined quantitatively and the critical water saturations have been calculated. The methodology has been developed

for the pore scale and applied to 3D experimental images of microstructures. The following main conclusions can be drawn:

- The pore-scale modified lattice Boltzmann model, implemented in the SCMPLBS module, can simulate realistically multiphase flow phenomena such as water–gas phase segmentation (Laplace's law) and variable wettability (contact angle).
- Water phase is found to cover the surface of solid phase and fill the smaller pores in the three-dimensional pore network preferentially. In contrast, the gas phase is found to occupy the central parts of large pores and to act as obstacle to the transport of ions.
- With reduction of water saturation level, the degree of water phase connectivity is found to decrease, initially gradually and then rapidly until a critical saturation is reached. For degree of the gas phase connectivity decreases with the saturation level in a more pronounced way than that of water phase.
- The water saturation level is not the sole key factor for the connectivity of the phases; the geometry of the porous network shaped by the arrangement of the solid phase plays also a critical role.
- The critical water saturation increases with the decrease of porosity. The critical water saturations for cement paste specimens with curing ages of 1, 7 and 28 days are 34%, 45% and 61%, respectively. These correspond to water-filled porosities of 9.3%, 8.5% and 8.3%, respectively, which is in a very good agreement with the existing knowledge that the percolation threshold of the capillary porosity in cementitious materials is around 9% porosity.

Acknowledgments

M Zhang and AP Jivkov gratefully acknowledge the support of BNFL for the Research Centre for Radwaste and Decommissioning and of EDF for the Modelling and Simulation Centre.

References

[1] Martys NS. Diffusion in partially-saturated porous materials. Mater Struct 1999;32(8):555–62.
[2] Therrien J, Bissonnette B. Early-age evolution of the mass transfer properties in mortar and its influence upon ultimate shrinkage. In: Baroghel-Bouny V, Aitcin PC, editors. Proceedings of International RILEM workshop on 'Shrinkage of Concrete – Shrinkage 2000'. Springer, Paris, France, p. 233–46.
[3] Chen TC, Yeung MR, Mori N. Effect of water saturation on deterioration of welded tuff due to freeze–thaw action. Cold Reg Sci Technol 2004;38(2–3):127–36.
[4] Cano-Barrita PFDJ, Marble AE, Balcom BJ, Carcia JC, Masthikin IV, Thomas MDA, et al. Embedded NMR sensors to monitor evaporable water loss caused by hydration and drying in Portland cement mortar. Constr Build Mater 2009;39:324–8.
[5] Zhang P, Wittmann FH, Zhao TJ, Lehmann E, Jin ZQ. Visualization and quantification of water movement in porous cement-based materials by real time thermal neutron radiography: theoretical analysis and experimental study. Sci China Technol Sci 2010;53(5):1198–207.
[6] Jusoh MA, Abbas Z, Lee KY, You KY, Norimi AM. Determination of moisture content in mortar at near relaxation frequency 17 GHz. Meas Sci Rev 2011;11(6):203–6.
[7] Ghandehari M, Vimer CS, Ioannou I, Sidelev A, Jin W, Spellane P. In situ measurement of liquid phase moisture in cement mortar. NDT&E Int 2012;45(1):162–8.
[8] Climent MA, de Vera G, Lopez JF, Viqueira E, Andrade C. A test method for measuring chloride diffusion coefficients through nonsaturated concrete: Part I. The instantaneous plane source diffusion case. Cem Con Res 2002;37(5):714–24.
[9] de Vera G, Climent MA, Viqueira E, Antón C, Andrade C. A test method for measuring chloride diffusion coefficients through partially saturated concrete: Part II. The instantaneous plane source diffusion case with chloride binding consideration. Cem Con Res 2007;32(7):1113–23.
[10] Care S, Derkx F. Determination of relevant parameters influencing gas permeability of mortars. Constr Build Mater 2011;25(3):1248–56.
[11] Åhs M, Nilsson L, Haha MB. A method to determine the critical moisture level for unsaturated transport of ions. Mater Struct 2013. http://dx.doi.org/10.1617/s11527-013-0167-5.
[12] Guimarães ATC, Climent MA, de Vera G, Vicente FJ, Rodrigues FT, Andrade C. Determination of chloride diffusivity through partially saturated Portland cement concrete by a simplified procedure. Constr Build Mater 2011;25(2):785–90.
[13] Mercado-Mendoza H, Lorente S, Bourbon X. Ionic aqueous diffusion through unsaturated cementitious materials – a comparative study. Constr Build Mater 2014;51(31):1–8.
[14] Janssen H, Derluyn H, Carmeliet J. Moisture transfer through mortar joints: a sharp-front analysis. Cem Con Res 2012;42(8):1105–12.
[15] Ye G. Experimental study and numerical simulation of the development of the microstructure and permeability of cementitious materials. PhD thesis, Delft University of Technology, The Netherlands; 2003.
[16] Dolado JS, van Breugel K. Recent advances in modelling for cementitious materials. Cem Con Res 2011;41(7):711–26.
[17] Zhang M. Multiscale lattice Boltzmann-finite element modelling of transport properties in cement-based materials. PhD thesis, Delft University of Technology, The Netherlands; 2013.
[18] van Breugel. Simulation of hydration and formation of structure in hardening cement-based materials. PhD thesis, Delft University of Technology, The Netherlands; 1991.
[19] Bentz DP. Guide to CEMHYD3D: a three-dimensional cement hydration and microstructure development modelling package. USA: NIST; 1997.
[20] Zhang M, He Y, Ye G, Lange DA, van Breugel K. Computational investigation on mass diffusivity in Portland cement paste based on X-ray computed tomography (μCT) image. Constr Build Mater 2012;27(1):472–81.
[21] Zhang M, Ye G, van Breugel K. Microstructure-based modelling of permeability of cementitious materials using multi-relaxation-time lattice Boltzmann method. Comput Mater Sci 2013;68:142–51.
[22] Zhang M, Ye G, van Breugel K. Multiscale lattice Boltzmann-finite element modelling of chloride diffusivity in cementitious materials. Part II: Simulation results and validation. Mech Res Commun 2014. http://dx.doi.org/10.1016/j.mechrescom.2014.01.001.
[23] Zhang M, Ye G, van Breugel K. Modelling of ionic diffusivity in non-saturated cement-based materials using lattice Boltzmann method. Cem Con Res 2012;42(11):1524–33.
[24] Zhang M, Ye G, van Breugel K. A numerical-statistical approach to determining the representative elementary volume (REV) of cement paste for measuring diffusivity. Mater Constr 2010;60(300):7–20.
[25] Shan X, Chen H. Lattice Boltzmann model for simulating flows with multiple phases and components. Phys Rev E 1993;47(3):1815–9.
[26] Shan X, Chen H. Simulation of non-ideal gases and liquid–gas phase transitions by lattice Boltzmann equation. Phys Rev E 1994;49(4):2941–8.
[27] Pan C, Hilpert M, Miller CT. Lattice-Boltzmann simulation of two-phase flow in porous media. Water Resour Res 2004;40(1):W01501.
[28] Qian YH, D'Humières D, Lallemand P. Lattice BGK models for Navier–Stokes equation. Europhys Lett 1992;17(6):479–84.
[29] Shan X, Doolen G. Multi-component lattice-Boltzmann model with interparticle interaction. J Stat Phys 1995;81(1–2):379–93.
[30] Yuan P, Schaefer L. Equations of state in a lattice Boltzmann model. Phys Fluids 2006;18(4):042101.
[31] Hoshen J, Kopelman R. Percolation and cluster distribution I. Cluster multiple labelling technique and critical concentration algorithm. Phys Rev B 1976;14(8):3438–45.
[32] Vu TH, Frizon F, Lorente S. Architecture for gas transport through cementitious materials. J Phys D: Appl Phys 2009;42:105501.
[33] Boher C, Frizon F, Lorente S, Bart F. Influence of the pore network on the hydrogen diffusion through blended cement pastes. Cem Concr Compos 2013;37:30–6.
[34] Zhang M, Morrison CN, Jivkov AP. A meso-scale site-bond model for elasticity: theory and calibration. Mater Res Innov 2014. http://dx.doi.org/10.1179/1432891714Z.000000000537.
[35] Zhang M, Jivkov AP. Microstructure-informed modelling of damage evolution in cement paste using a site-bond method. Constr Build Mater, submitted for publication.